



1 **Investigating the response of China's surface ozone**
2 **concentration to the future changes of multiple factors**

3

4 Jinya Yang¹, Yutong Wang¹, Lei Zhang^{1,2}, Yu Zhao^{1,2*}

5

6 1. State Key Laboratory of Pollution Control and Resource Reuse, School of
7 Environment, Nanjing University, 163 Xianlin Rd., Nanjing, Jiangsu 210023, China

8 2. Jiangsu Collaborative Innovation Center of Atmospheric Environment and
9 Equipment Technology (CICAEET), Nanjing University of Information Science and
10 Technology, Jiangsu 210044, China

11

12 *Corresponding author: Yu Zhao

13 Phone: 86-25-89680650; email: yuzhao@nju.edu.cn

14



15 **Abstract**

16 Climate change and associated human response are supposed to greatly alter
17 surface ozone (O_3), an air pollutant generated through photochemical reactions
18 involving both anthropogenic and biogenic precursors. However, a comprehensive
19 evaluation of China's O_3 response to these multiple changes has been lacking. We
20 present a modelling framework under Shared Socioeconomic Pathways (SSP2-45),
21 incorporating future changes in local and foreign anthropogenic emissions,
22 meteorological conditions, and BVOCs emissions. From the 2020s to 2060s, daily
23 maximum 8-hour average (MDA8) O_3 concentration is simulated to decline by 7.7 ppb
24 in the warm season (April-September) and 1.1 ppb in non-warm season (October-
25 March) over the country, with a substantial reduction in exceedances of national O_3
26 standards. Notably, O_3 decreases are more pronounced in developed regions such as
27 BTH, YRD, and PRD during warm season, with reductions of 9.7, 14.8, and 12.5 ppb,
28 respectively. Conversely, in non-warm season, the MDA8 O_3 in BTH and YRD will
29 increase by 5.4 and 3.4 ppb, partly attributed to reduced NO_x emissions and thereby
30 weakened titration effect. O_3 pollution will thus expand into the non-warm season in
31 the future. Sensitivity analyses reveal that local emission change will predominantly
32 influence future O_3 distribution and magnitude, with contributions from other factors
33 within $\pm 25\%$. Furthermore, the joint impact of multiple factors on O_3 reduction will be
34 larger than the sum of individual factors, due to changes in the O_3 formation regime.
35 This study highlights the necessity of region-specific emission control strategies to
36 mitigate potential O_3 increases during non-warm season and under climate penalty.

37 **1 Introduction**

38 Surface ozone (O_3) is a secondary air pollutant generated by photochemical
39 reactions in the presence of two main kinds of precursors NO_x ($NO_x=NO+NO_2$) and
40 volatile organic compounds (VOCs). It has been reported to be a non-negligible threat
41 to both human health and crop yield, and also a short-lived climate forcer with



42 warming effect (Finlaysonpitts and Pitts, 1997; Jerrett et al., 2009; Avnery et al., 2011;
43 von Schneidmesser et al., 2015; Tai and Val Martin, 2017; Feng et al., 2022). Given
44 the abundant emissions of anthropogenic NO_x and VOCs, China has suffered from
45 extremely high and continuously increasing O₃ pollution from 2013 to 2019 with the
46 peak season daily maximum 8-hour average (MDA8) O₃ concentration over 95 μg m⁻³.
47 The rising trend has been reversed since 2020, along with the national annual NO_x and
48 non-methane VOCs (NMVOCs) emissions reduced by 28.3 % and 3.8 %, respectively
49 during 2013–2020 (Zheng et al., 2018; Xiao et al., 2022; Liu et al., 2023; Wang et al.,
50 2023). However, current O₃ concentration over China is still much higher than the
51 global air quality guidelines (60 μg m⁻³ for the averaged peak season MDA8 O₃, WHO,
52 2021). This presents a great challenge for the country to meet the criteria for public
53 health welfare in the future (Feng et al., 2023; Jiang et al., 2023).

54 In addition to the anthropogenic driver, studies also addressed the roles of
55 meteorological factors, biogenic VOCs (BVOCs) emissions and transboundary
56 transport of pollutants on O₃ enhancement in China (Monks et al., 2015; Lu et al., 2019;
57 Cao et al., 2022; Wang et al., 2022; Weng et al., 2022; Jiang et al., 2023).
58 Meteorological factors, including temperature, humidity, wind, etc., influence the
59 chemical reactions associated with O₃ production and elimination, and the
60 transportation of O₃ precursors (Gong and Liao, 2019). The changed meteorology was
61 estimated to enhance the summer MDA8 O₃ concentration by 1.4 ppb yr⁻¹ during 2013–
62 2019 in the North China Plain (NCP), nearly half of the overall O₃ growth of 3.3 ppb
63 yr⁻¹ (Li et al., 2020a). BVOCs refer to VOCs emitted from terrestrial ecosystems and
64 possess high reactivity in atmospheric chemical processes, mainly including isoprene,
65 monoterpenes and sesquiterpene (Wu et al., 2020). Cao et al. (2022) reported that
66 BVOCs emissions in summer 2018 enhanced 8.6 ppb MDA8 O₃ averaged over China
67 with the highest contribution over 30 ppb in southern China. Moreover, O₃ and its
68 precursors could be transported over long distance, and transboundary foreign
69 anthropogenic emissions were estimated to contribute 2–11 ppb to near surface O₃ in



70 China (Ni et al., 2018; Han et al., 2019).

71 In the context of future global change, substantial but uncertain changes will occur
72 in economy, climate and land cover. According to the Sixth Assessment Report of
73 Intergovernmental Panel on Climate Change (IPCC AR6 report), the global surface
74 temperature will increase 0.2–3.7 °C till 2100 under different scenarios compared to
75 2015 (IPCC, 2021, 2022). As a result, unfavorable meteorological extremes, such as
76 high temperature extremes and ecological drought events, will be more frequent and
77 intense (Hong et al., 2019; Porter and Heald, 2019; IPCC, 2021), leading to the
78 deterioration of air quality named as climate penalty. To conquer the climate change
79 and resulting air quality deterioration, a series of measures will be implemented, such
80 as accelerating the transition to clean energy, upgrading industrial production
81 technologies and strengthening pollution control measures. Attributable to these
82 changes, annual mean surface O₃ in East Asia was projected to change by –13.9–6.1
83 ppb till 2100 compared to 2015 (IPCC, 2021). However, limited by the coarse
84 resolution of earth system model and the lack of consideration of the regional measures
85 for reducing air pollution and carbon emissions, global estimation is insufficient for
86 understanding how O₃ pollution in China will respond to the complex future change.

87 There have been some studies on how the above-mentioned changes will affect
88 future O₃ level in China. Hong et al. (2019) reported that the 1-hour maximum O₃ in
89 April to September will be enhanced by 2–8 ppb within large areas of China under
90 RCP4.5 (representative concentration pathways 4.5, van Vuuren et al., 2011) scenario
91 from the 2010s to 2050s. Under high-forcing scenarios, Li et al. (2023) projected the
92 climate-driven O₃ concentration in the 2100s and found that O₃ concentration in
93 southeast China would increase 5–20 % compared to the 2020s by a machine learning
94 method. A warming climate should enhance the O₃ level, given the increasing
95 frequency of atmospheric stagnation and heat waves (Hong et al., 2019; Wang et al.,
96 2022; Gao et al., 2023; Li et al., 2023). The effect of anthropogenic emission change
97 on China's O₃ level has been estimated by studies under different scenarios. Zhu and



98 Liao (2016) applied global emission estimates under RCPs, and found that the
99 maximum growth of annual mean O₃ would be 6–12 ppb during 2000–2050 under
100 different scenarios. Using the Dynamic Projection model for Emissions in China
101 (DPEC) that better includes local information of energy transition and emission
102 controls (Cheng et al., 2021b), Xu et al. (2022) reported that the joint impact of climate
103 change and emission reduction would reduce the annual MDA8 O₃ concentration to
104 63.0 µg m⁻³ under ambitious scenario of carbon neutrality. Biogenic emission change
105 is another factor influencing future O₃ (Chen et al., 2009; Andersson and Engardt, 2010;
106 Harper and Unger, 2018; Wang et al., 2020). Liu et al. (2019) predicted a 24 % growth
107 of BVOCs emissions driven by climate change under RCP8.5 from 2015 to the 2050s,
108 resulting in a variation of daily 1-h maximum O₃ concentration ranging from –10.0 to
109 19.7 ppb across different regions in China.

110 Limitations exist in current studies, which prevent comprehensive assessment and
111 understanding of the joint impacts of future changes of multiple factors on China's O₃
112 pollution. Firstly, the above estimations mainly focused on the influence of future
113 changes on summertime or annual average O₃ concentration. As China's O₃ pollution
114 has been reported to spread into spring and fall, it is of great importance to separate the
115 impacts on warm (April to September, the six months with heaviest O₃ pollution for
116 most part of China, Liu et al., 2023) and non-warm season O₃ (October to March),
117 considering the diverse air pollution sources and O₃ formation sensitivity to precursors
118 for different seasons (Li et al., 2021; Wang et al., 2023). In addition, the rising
119 frequency of extreme weathers and declining anthropogenic emissions will further
120 influence the possibility of extreme O₃ events, which has been scarcely discussed.
121 Secondly, to restrain global warming, China has made a national commitment to
122 achieving “carbon neutrality” by 2060 (Shi et al., 2021), and accordingly launched a
123 series of energy and climate action plans to reduce greenhouse gas emissions. These
124 actions will also cause substantial reductions in air pollutant emissions, but have not
125 been fully included in existing predictions of global emissions (Tong et al., 2020; Cheng



126 et al., 2021b). Large bias will then be caused in the simulation of anthropogenic-
127 induced future changes of air quality, with a less realistic estimate of local emission
128 path (Cheng et al., 2021a). Due to probably faster decline of emissions in China but
129 slower in surrounding countries in the future, the contributions of transboundary
130 emissions on China's O₃ can be greatly changed and has not yet been considered.
131 Thirdly, BVOCs emissions will not only be affected by meteorological factors but also
132 by land use and land cover change (Penuelas and Staudt, 2010; Szogs et al., 2017; Wang
133 et al., 2021a). Future land management will change due to socio-economic development
134 and necessary actions as climate change response, and the changed shares of forest,
135 cropland and grassland will alter the magnitude and distribution of BVOCs emissions
136 and thereby affect O₃ concentration (Hurt et al., 2020; Liao et al., 2020; Liu et al.,
137 2022). Finally, the existing evaluations were conducted separately for individual
138 influencing factors, with diverse methods and data. The interactions between different
139 factors were seldom included in existing analyses, and the relative contributions of
140 multiple factors were difficult to be evaluated or compared. Relevant studies have been
141 conducted in developed countries (Gonzalez-Abraham et al., 2015), and are still lack in
142 China.

143 In this study, we evaluate the complex influence of future changes of multiple
144 factors on surface O₃ concentration in China within a uniform framework. The
145 evaluation is conducted from the perspectives of seasonal, regional and extreme events
146 of O₃ pollution. Four factors are included in the analyses, i.e., meteorological conditions,
147 local anthropogenic emissions, BVOCs emissions, and anthropogenic emissions from
148 surrounding foreign countries. The analyses are conducted based on a series of
149 sensitivity experiments in numerical modelling of future air quality, and up-to-date
150 input data from multiple sources are utilized in the model (see details in next section).
151 We provide a comprehensive perspective on the spatiotemporal change of China's O₃
152 pollution till the 2060s, under a moderate way SSP2 of Shared Socioeconomic
153 Pathways (SSPs, Riahi et al., 2017) and a midrange mitigation scenario RCP4.5, a



154 scenario at the middle of the socio-economic developing way with radiative forcing at
155 4.5 W m^{-2} nominally by 2100 (Meinshausen et al., 2020). The outcomes highlight the
156 regional and seasonal heterogeneity of O_3 pollution risks driven by complex future
157 change of multiple factors, and support strategy design of O_3 pollution alleviation with
158 specific principles, targets and action pathways.

159 **2 Data and Methods**

160 **2.1 Main framework and research domain**

161 The simulation framework incorporates the Weather Research and Forecasting
162 model (WRF, version 3.7.1) to the generate hourly meteorological fields, the Model of
163 Emissions of Gases and Aerosols from Nature (MEGAN, version 2.1) to calculate
164 gridded BVOCs emissions, and the Community Multiscale Air Quality model (CMAQ,
165 version 5.2) to simulate O_3 concentration. BVOCs emission calculation and air quality
166 simulations are driven by meteorological fields of 2018–2022 (the 2020s, representing
167 the current situation) and 2058–2062 (the 2060s, representing the future situation). All
168 simulation results are averaged over a period of five years to mitigate the influence of
169 interannual variability of meteorology. The modelling domain, same for WRF,
170 MEGAN and CMAQ, covers East Asia, most areas of South Asia and Central Asia, and
171 part of Southeast Asia and North Asia (Figure 1). It applies the Lambert Conformal
172 Conic projection centered at (110° E , 34° N), and the horizontal resolution is $27 \text{ km} \times 27$
173 km , with 303×203 grids. The target area, Chinese mainland, includes 31 provincial-
174 level administrative regions (excluding Hong Kong, Macao and Taiwan). Eight
175 geographical regions are defined, and locations of the three regions with dense
176 population and relatively heavy air pollution are also shown in Figure 1, namely BTH
177 (Beijing-Tianjin-Hebei), YRD (Yangtze River Delta) and PRD (Pearl River Delta).

178 **2.2 Data sources and processing methods**

179 We use the bias-corrected RCP4.5 output of the National Center for Atmospheric



180 Research's Community Earth System Model (NCAR CESM) as initial and boundary
181 conditions for WRF (Monaghan et al., 2014). A ten-year dynamic downscaling
182 simulation for 2018–2022 and 2058–2062 is conducted. Note we do not utilize the real-
183 time reanalysis data to drive the simulation of the 2020s, in order to minimize the
184 systematic error between the simulation driven by real meteorological conditions (for
185 current simulations) and climate projection (for future simulations),

186 The BVOCs emissions are basically determined by meteorology and vegetation.
187 The meteorological conditions are supplied by WRF. The vegetation data, including
188 leaf area index (LAI), plant functional types (PFTs) and emission factors (EFs) of each
189 PFT, are determined for 2020 and 2060. Gridded LAI data for 2020 are obtained from
190 Global Land Surface Satellite product (Liang et al., 2021), and those for 2060 under
191 SSP2-45 scenario are downscaled from the daily CESM2 output of Coupled Model
192 Intercomparison Project Phase 6 (CMIP6). PFTs data for 2020 are derived from
193 MCD12C1 product of Moderate-Resolution Imaging Spectroradiometer (MODIS)
194 dataset and mapped to the 16 types required for MEGAN following Liao et al. (2020).
195 The PFTs data for 2060 in China are obtained from Liao et al. (2020) under SSP2-45
196 scenario, with other regions maintaining those of 2020. EFs for each PFT are taken
197 from Guenther et al. (2012).

198 Anthropogenic emissions for Chinese mainland are obtained from the Multi-
199 resolution Emission Inventory for China (MEIC,
200 http://meicmodel.org.cn/?page_id=560) for 2020, and DPEC version 1.1 under SSP2-
201 45 incorporating the best available end-of-pipe pollution control technologies for 2060.
202 Emissions outside Chinese mainland are obtained from CMIP6 dataset under SSP2-45
203 scenario (O'Neill et al., 2016; Gidden et al., 2019). The spatial and temporal
204 distributions of emissions outside Chinese mainland are assumed the same as those in
205 MIX Asian emission inventory (Li et al., 2017). The speciation profiles of NMVOCs
206 are taken from MIX as well. Supplementary Figure S1 shows the emissions of two main
207 precursors of O₃ by year and region. The NO_x and NMVOCs emissions for Chinese



208 mainland were estimated to decline 58 % and 51 % from 2020 to 2060, respectively,
209 much faster than those of surrounding areas within the modelling domain (8 % and 14 %
210 respectively). In particular, the NO_x emissions would decline 57–62 % for the three
211 developed regions BTH, YRD and PRD, while the reductions of anthropogenic
212 NMVOCs would vary a lot among regions (36 %, 49 % and 60 % for BTH, YRD and
213 PRD, respectively).

214 Carbon Bond 2005 (CB05, Yarwood et al., 2005) is adopted as the gas-phase
215 chemical mechanism and the sixth-generation CMAQ aerosol module AERO6 (Appel
216 et al., 2013) as aerosol chemistry mechanism. The initial and boundary conditions are
217 set by default clean air conditions in CMAQ, and the first 10 days for each year are
218 determined as the spin-up period to minimize the effects of initial and boundary
219 conditions.

220 **2.3 Simulation cases**

221 Six cases of CMAQ simulations are conducted to investigate the impacts of future
222 change of the four factors on O₃ concentration in China (Table 1). Cases 1 and 2
223 represent the current (2020s) and future (2060s) baseline, respectively, and the
224 difference between them indicates the joint effect of the future changes of multiple
225 factors. Each of Cases 3–6 applies the prediction for 2060s for one specific factor but
226 keeps the remaining factors at current condition (2020s). Thus, the difference between
227 each of those four cases and Case 1 indicates the impact of individual factor, including
228 meteorological conditions (Case 3), domestic anthropogenic emissions (Case 4),
229 BVOCs emissions (Case 5) and anthropogenic emissions of surrounding countries
230 (Case 6). Each case contains a five-year (2018–2022 or 2058–2062) WRF-MEGAN-
231 CMAQ simulation driven by the varying meteorological conditions for individual years,
232 and the five-year average of simulated O₃ concentrations is adopted for further analyses.

233 **2.4 Model performance**

234 To evaluate the model performance, we conduct a comparative analysis between



235 simulations and observations for meteorological factors and O₃ concentrations, as well
236 as an intercomparison for BVOCs estimates between different studies.

237 We first examine the capability of downscaled CESM climate projections in
238 capturing the meteorological conditions of the 2020s. We applied the meteorological
239 data from the National Climate Data Center (NCDC, archived at <https://quotsoft.net/air>)
240 in 2020, and the statistical metrics are presented in Supplementary Table S1. The
241 modeled temperature at 2 m (T2) is in good spatiotemporal agreement with the
242 observations, with the correlation coefficient (R) of 0.96 and index of agreement (IOA)
243 of 0.98. The relative humidity (RH) is also well predicted with R and IOA at 0.78 and
244 0.88, respectively. The model shows an overestimation on the wind speed by 1.41 m
245 s⁻¹, which is also reported by Hu et al., (2022). The correlation coefficients of wind
246 speed and direction are higher than 0.5. Overall, the modeled meteorological fields have
247 basically captured the conditions in China and are appropriate for subsequent MEGAN
248 and CMAQ simulations.

249 For BVOCs emissions, we compare our estimates for the 2020s with previous
250 studies, as summarized in Supplementary Table S2. The total BVOCs, isoprene and
251 terpenes emissions in this study are estimated at 33.55, 21.08 and 3.30 Tg yr⁻¹,
252 respectively, and are comparable to other studies. In particular, our estimate is larger
253 than others except for Li et al. (2020b) for isoprene, while smaller than others except
254 for Wu et al. (2020) for terpenes. The differences between studies might result from the
255 diverse strategies of mapping PFTs from the original satellite products and the
256 difference between downscaled climate conditions and the real meteorological fields.

257 We apply the observed MDA8 O₃ concentration data from the national network of
258 China Ministry of Ecology and Environment (archived at <https://quotsoft.net/air>) to
259 evaluate CMAQ performance. As shown in Supplementary Figure S2, the simulation
260 could capture the spatiotemporal distribution of surface MDA8 O₃ concentration for the
261 whole country and specific O₃ pollution hot spots, e.g., BTH and eastern Sichuan
262 province with their surrounding areas. The statistical metrics of the comparisons



263 between the simulated and observed monthly average MDA8 O₃ concentration of 2020s
264 are summarize in Supplementary Table S1. The normalized mean biases (NMB) are
265 calculated at 14.12 % and 10.90 % for warm and non-warm season, and R values at
266 0.71 and 0.32, respectively. Even with a slight overestimation, the reliability of our
267 simulation is comparable to most previous studies in China, with a better performance
268 in the warm season (Hu et al., 2016; Lu et al., 2019; Gao et al., 2020; Yang and Zhao,
269 2023).

270 **3 Results and Discussions**

271 **3.1 Future change of meteorology and BVOCs emissions**

272 The downscaled changes in the meteorological factors from the 2020s to 2060s
273 (SSP2-45 scenario) are shown in Figure 2, including temperature, RH and wind speed
274 (WS). The changes are analyzed separately for April–September (warm season) and
275 October–March (non-warm season). For the warm season, daily maximum temperature
276 at 2 m (T-max) will increase across China with an average change of 1.0 °C, and the
277 minimum and maximum changes are found in Tibetan Plateau at 0.1 °C and in
278 Heilongjiang province at 2.1 °C, respectively. The RH will decrease slightly by –0.6 %
279 for the whole country, with the changes for most areas within the range between –3 %
280 and 0 % except for some areas of Northwestern China, Southwestern China, and
281 Tibetan Plateau (see the region definitions in Figure 1). The growing T-max and
282 declining RH will enhance the photochemical production of O₃ and BVOCs emissions.
283 For the non-warm season, the national average growth of T-max will be smaller at 0.2 °C
284 and some areas in Northeastern, Northern and Eastern China will even experience a
285 decline ranging from –1.8 to 0 °C. The RH will change diversely across the country,
286 ranging from –6.0 to 6.3 %. Very limited change in WS will occur, ranging from –0.1
287 to 0.2 m s⁻¹ in most areas of the country. The spatial distribution of downscaled future
288 meteorological field changes is generally in agreement with those predicted by Hong et
289 al. (2019) and Hu et al. (2022). Some discrepancies in temperature and wind speed



290 change of non-warm season between studies result from the different choices of base
291 year and parameterization schemes of WRF.

292 Table 2 shows China's BVOCs emissions of the 2020s and 2060s (SSP2-45
293 scenario) estimated with MEGAN, as well as the BVOCs emission intensity (emissions
294 per unit area) for the three developed regions. The emissions will increase from 33.6
295 Tg yr⁻¹ for the 2020s to 43.4 Tg yr⁻¹ for the 2060s. The growth rates in BTH, YRD and
296 PRD are predicted to be 22.4 %, 23.9 % and 23.0 %, respectively, smaller than that for
297 the whole country (29.2 %). The spatial distributions of BVOCs emissions for the 2020s
298 and the changes from the 2020s to 2060s, are shown in Supplementary Figure S3. Areas
299 all over China will experience the growth of BVOCs emissions, and it will be more
300 prominent in areas with high vegetation coverage (e.g., Southern and Southwestern
301 China) rather than urban areas. The growth of BVOCs emissions will enhance the
302 contribution of natural sources to O₃ formation, especially along with declining
303 anthropogenic emissions in the future (Penuelas and Llusia, 2003; Riahi et al., 2017;
304 Gao et al., 2022).

305 **3.2 Response of surface O₃ concentration to combined future changes**

306 Figure 3 illustrates the spatial distributions of MDA8 O₃ concentrations for the
307 warm and non-warm seasons of the 2020s and 2060s (SSP2-45 scenario), as well as the
308 differences between the two periods. Briefly, future changes of the four factors under
309 SSP2-45 are estimated to jointly reduce MDA8 O₃ by 7.7 and 1.1 ppb in the warm and
310 non-warm season, respectively, while the O₃ responses to future changes will differ by
311 region.

312 In the warm season of the 2020s (Figure 3a), the nationwide average MDA8 O₃
313 concentration is simulated at 57.3 ppb, and those of BTH, YRD and PRD are 73.7, 68.7
314 and 52.3 ppb, respectively. Hot spots of O₃ pollution, with average MDA8 O₃ over 75
315 ppb, are mainly located in Northern China and Sichuan province. The pattern is
316 predicted to persist into the 2060s (Figure 3b), with a decline in both the severity and
317 size of highly polluted regions. The nationwide MDA8 O₃ concentration will decline



318 13.4 % to 49.6 ppb, and that in most areas of China will be within the range of 37.5–
319 67.5 ppb. The highest concentration will be lower than 75 ppb for the two hotspots of
320 Northern China and Sichuan. BTH will remain as the most O₃-polluted area in warm
321 season, with the O₃ concentration at 63.9 ppb (13.3 % smaller than the 2020s), while
322 that of YRD and PRD will decrease to 53.9 (21.5 %) and 39.8 ppb (23.9 %),
323 respectively. O₃ concentration in the developed regions will decline faster than or
324 roughly the same as that for the whole country. The reductions in MDA8 O₃ from 2020s
325 to 2060s will be 10–20 ppb for Northern, Eastern, Central and Southern China and 0–
326 10 ppb for Northeastern and Northwestern China as well as the Tibetan Plateau (Figure
327 3c). Notably, some areas in Sichuan are expected to experience a substantial decline of
328 MDA8 O₃ over 20 ppb.

329 O₃ concentration of the non-warm season is simulated to be much lower than that
330 of the warm season. The 2020s average MDA8 O₃ is 48.4 ppb, ranging from 30.0 to
331 67.5 ppb in most areas of China (Figure 3d). Different from the warm season in which
332 highest concentration is found for Northern China and Sichuan, the Southern and
333 Southwestern parts of China suffer the highest O₃ level for the non-warm season. A
334 general west-to-east and south-to-north gradient is found for MDA8 O₃, with the lowest
335 concentration found in Northern and Northeastern China. The concentrations in BTH
336 and YRD are simulated at 33.8 and 45.1 ppb, respectively, much lower than that of
337 PRD (58.9 ppb). Relatively high temperature during even the non-warm season is
338 expected to expand the O₃ pollution period in Southern China. Resulting from complex
339 change of multiple factors, the national average MDA8 O₃ concentration in the non-
340 warm season of 2060s will decrease slightly to 47.3 ppb under SSP2-45, and that in
341 most regions will be within the range of 37.5–52.5 ppb except for some areas in
342 Northeastern China and Tibetan Plateau (Figure 3e). The MDA8 O₃ concentrations of
343 the three developed regions will become closer at 39.3, 48.4 and 51.6 ppb for BTH,
344 YRD and PRD, respectively. As illustrated in Figure 3f, MDA8 O₃ is predicted to
345 increase in BTH and YRD and the surrounding areas, with the growth mostly ranging



346 0–15 ppb. In other areas (especially in Southern China), the concentration will decrease
347 in the non-warm season by –15 to –5 ppb. As a result of the increased O₃ in the less
348 polluted Eastern and Northern China and decreased O₃ in the more polluted
349 Southwestern and Southern parts, the 2060s regional disparity in the non-warm season
350 O₃ pollution will get smaller compared to the 2020s (Figure 3d and 3e).

351 To further explore the temporal pattern of O₃ level in the future, we compare the
352 monthly average MDA8 O₃ in the 2020s and 2060s under SSP2-45 for the whole
353 country and three developed regions (Figure 4 and Supplementary Figure S4). For the
354 whole country (Figure 4a), the changes of monthly average MDA8 O₃ from 2020s to
355 2060s are estimated to range from –3.2 to –10.7 ppb in the warm season but less
356 prominent in the non-warm season (from –2.7 to 0.9 ppb). Along with the more
357 reduction in summertime (June, July and August), in particular, the periods with the
358 highest O₃ concentration will expand into spring (March) and fall (October), as
359 presented in Supplementary Figure S4. For the three regions, a greater decline in O₃
360 concentration is found in the warm season while a smaller or even a growth is found in
361 the non-warm season. For BTH (Figure 4b), the monthly MDA8 O₃ concentrations
362 range between 24.7 and 88.4 ppb in the 2020s with a clear difference between the warm
363 and non-warm season. This pattern will remain in the 2060s with smaller difference
364 between months (30.6–70.2 ppb). The temporal change pattern of YRD is similar to
365 that in BTH, with decline in the warm season and growth in the non-warm season
366 (Figure 4c). The shift of O₃ pollution from the warm towards the non-warm season is
367 more prominent in the PRD, the only region where O₃ concentration of all the months
368 in 2060s is predicted to decline (Figure 4d). Different from BTH and YRD, as
369 mentioned above, higher O₃ concentrations during spring and autumn and lower in
370 summer (due to the abundant summertime precipitation and high humidity) are found
371 for PRD in the 2020s (Gao et al., 2020; Han et al., 2020). With great O₃ decline in the
372 warm season, the periods experiencing peak O₃ pollution are predicted in the non-warm
373 season of the 2060s, predominantly between October and March (Supplementary



374 Figure S4).

375 **3.3 Identifying surface O₃ response to individual factors**

376 **3.3.1 Local anthropogenic emission change**

377 Figure 5 shows the influences of changes of each individual factors (local
378 anthropogenic emissions, meteorological conditions, BVOCs emissions, and
379 anthropogenic emissions from surrounding countries) on the warm and non-warm
380 season O₃ concentrations. Out of the four, the change of local anthropogenic emissions
381 is predicted to be the most influential factor, resulting in a national average decline of
382 7.2 and 0.8 ppb for the warm and non-warm season, respectively (Figure 5a and 5e). In
383 the warm season, the emission reduction will play a positive role in reducing O₃
384 pollution in most areas of China, and the decrease will exceed 10 ppb across Northern,
385 Eastern, Central, Southern and part of Southwestern China. In the non-warm season,
386 emission reduction will have contrasting effects on MDA8 O₃ levels in the north and
387 south part of China, enhancing MDA8 O₃ by 0–15 ppb for the former while restraining
388 it by 0–10 ppb for the latter. Especially, the emission reduction is predicted to elevate
389 the O₃ concentration by 5.9 and 4.0 ppb for BTH and YRD respectively.

390 Supplementary Figure S5 shows the relative emission reductions from 2020s to
391 2060s by region. Under SSP2-45 scenario, the reductions of NO_x and VOCs emissions
392 will range from 35.6 % to 63.6 % for different regions, and VOCs emission reduction
393 will be less than that of NO_x except for PRD. As the NO_x-limited regime for O₃
394 formation (i.e., O₃ is more sensitive to NO_x emission change) occurs more frequently
395 in the warm season while the VOC-limited regime more in the non-warm season, the
396 larger decline of NO_x emissions than VOCs should be more effective in restraining the
397 warm season O₃ pollution but has less benefit or even negative effect in the non-warm
398 season (Sillman and He, 2002). Wintertime of NCP and YRD have been reported under
399 the VOC-limited regime and the excessive NO_x emissions play an important role in
400 removing O₃ by titration effect (Jin and Holloway, 2015; Li et al., 2021; Wang et al.,



401 2021b). This may explain the MDA8 O₃ increase during the non-warm season with
402 insufficient reduction of VOCs (35.6 % and 49.5 %) but sharp reduction of NO_x of 53.4 %
403 and 60.3 % for NCP and YRD, respectively. Supplementary Figure S6 shows the
404 monthly variation of O₃ and odd oxygen (O_x, O_x=O₃+NO₂, representing the real
405 photochemical production potential of O₃ considering the titration effect) in the 2020s
406 and 2060s. It should be noted that the growth of O₃ in the non-warm season in 2060s
407 for BTH and YRD will be accompanied by minimal change of O_x, while the declines
408 of O₃ and O_x will appear simultaneously in the warm season for the three regions and
409 in non-warm season for PRD. This indicates that the growth of non-warm season O₃ in
410 BTH and YRD should result partly from NO_x reduction and thereby weakened NO
411 titration, as titration is a key pathway of O₃ loss when the chemical reactivity is
412 relatively low in winter (Gao et al., 2013; Akimoto and Tanimoto, 2022). The
413 differentiated O₃ responses to precursor reduction between YRD and PRD have also
414 been detected during the COVID-19 breakout period. With the O₃ isopleth plots, Wang
415 et al. (2021b) illustrated that 40–60 % reduction of NO_x and VOCs enhanced the O₃
416 formation in YRD under the VOC-limited regime but suppressed O₃ in PRD under the
417 transitional regime (a regime between NO_x- and VOC-limited). Therefore, VOCs
418 emission controls should be better addressed for O₃ pollution alleviation when it
419 expands to non-warm season in the future.

420 **3.3.2 Meteorological condition change**

421 As shown in Figure 5b and 5f, the influence of meteorological change exhibits
422 different patterns for the warm and non-warm season.

423 In the warm season, meteorological change due to global warming will play a
424 positive role on O₃ formation in most of China, with the enhancement within 0–4 ppb,
425 but it will reduce the O₃ level in remote areas like Tibetan Plateau. The national average
426 growth will be 0.3 ppb and that for YRD, PRD and BTH will be 1.9, 0.7, and 0.3 ppb,
427 respectively. The response of O₃ to meteorological change is associated with some
428 specific variables (Hong et al., 2019). For example, the great enhancement of O₃ in



429 YRD might be attributable to a hotter, dryer and more stable atmosphere with growth
430 of T-max (over 0.6 °C) and decline of RH and WS (Figure 2). The result is similar to
431 Hong et al. (2019), which reported a change of 2–8 ppb of daily 1-hour maximum O₃
432 concentration for the peak season from the 2010s to 2050s under RCP4.5. In addition,
433 the declining O₃ in Tibetan Plateau and the surrounding areas might result partly from
434 the weakened long-range transport of peroxyacetyl nitrate (PAN, the principal NO_x
435 reservoir) from the polluted areas (Fischer et al., 2014). Driven by the elevated
436 temperature, PAN from relatively polluted regions will undergo stronger thermal
437 decomposition locally, thus fail to be transported far away to the remote regions to
438 promote O₃ formation (Liu et al., 2013; Lu et al., 2019).

439 The influence of meteorological change on O₃ production is predicted to be much
440 smaller for the non-warm season, with the magnitude within ±1 ppb in most areas and
441 nationwide average at −0.2 ppb. In the three developed regions, the changes are
442 predicted to range from −0.4 to 0.3 ppb, with little regional difference. The limited
443 influence might be attributable to the modest change in temperature and RH in the non-
444 warm season.

445 **3.3.3 BVOCs and surrounding anthropogenic emission change**

446 Compared to domestic emissions, change of BVOCs emissions and anthropogenic
447 emissions from surrounding countries will have a less influence (within ±3 ppb) on
448 surface O₃ concentration in China. BVOCs change tends to enhance O₃ while foreign
449 emission change tends to restrain it in most areas (Figure 7).

450 The growing BVOCs emissions due to vegetation and climate change is estimated
451 to enhance O₃ concentration by 0–3 ppb in the most areas of China, with a larger
452 influence of 0.6 ppb in the warm season than that of 0.3 ppb in the non-warm season
453 across the country (Figure 5c and 5g). In the warm season, relatively large growth of
454 O₃ concentration will occur in BTH at 2.1 ppb, and those of YRD and PRD will be 1.5
455 and 1.0 ppb, respectively. The abundant NO_x emissions in BTH are expected to result
456 in a larger O₃ concentration response to BVOCs emission change than YRD and PRD,



457 even the BVOCs emission change of BTH will be smaller than the other two regions
458 (Table 2). The result is in agreement with other numerical simulation experiments. Liu
459 et al. (2019) reported a prominent O₃ enhancement even with a low BVOCs emission
460 rate under RCP8.5, in a NO_x-abundant environment. In the remote areas like Tibetan
461 Plateau and part of Northeastern China, the increased BVOCs will remove O₃ due to
462 the isoprene ozonolysis in low-NO_x environment (Hollaway et al., 2017; Zhu et al.,
463 2022). In general, regions with higher O₃ pollution levels and NO_x emissions will suffer
464 more risk of O₃ growing from rising BVOCs emissions in the future.

465 Most areas of China will benefit from the foreign emission change in terms of O₃
466 pollution alleviation (Figure 5d and 5h). An exception is Tibetan Plateau and its
467 surrounding areas, which will be affected by the elevated emissions of NO_x and VOCs
468 from South Asia under SSP2-45. Limited by the range of pollutant transport, greater
469 impacts will be found for coastal and border areas and less for inland areas (Ni et al.,
470 2018). Larger O₃ changes in the three developed regions are predicted than that of the
471 whole country, benefitting from the precursor emission reduction in East Asia and
472 Southeast Asia.

473 **3.4 The relationship between the joint and separate effects of multiple factors**

474 Figure 6 summarizes the contributions of individual factors to the total O₃ change
475 by region and season. Due to the nonlinear response of O₃ to multi-factor changes, the
476 aggregated contribution of the four factors does not equal to the joint contribution (i.e.,
477 there exist gaps between the difference of the 2020s and 2060s and the aggregated
478 contribution of four factors).

479 The varying domestic anthropogenic emissions are predicted to dominate the
480 change of the future O₃, with a relative contribution ranging from 75 % to 117 % for
481 different regions and seasons. The relative contributions of the other three factors are
482 estimated to be limited within ±25 % at national and regional level. Among different
483 regions, YRD will be more affected by climate change with the contribution of -13 %
484 and -12 % for the warm and non-warm season, respectively, far greater than that of



485 BTH and PRD (−6 % to 0 %). BTH will be more affected by BVOCs emission change
486 than other regions in the warm season (−21 %), while YRD and PRD will be more
487 affected in the non-warm season with the relative contributions of 17 % and −20 %,
488 respectively. Little regional difference is found for the relative contributions of foreign
489 emission change.

490 To better understand the regional and seasonal differences of the relative
491 contributions of future changes to O₃ concentration, we examine the nonlinear response
492 of O₃ to precursor change in the three developed regions. We follow Chen et al. (2021)
493 and Schroeder et al. (2017), and conduct a fit of lognormal distribution for the
494 relationship of modeled hourly O₃ and NO₂ concentrations, as shown in Figure 7. The
495 data points on the left of the turning point of fitted curve suggest a NO_x-limited regime
496 while on the right a VOC-limited regime, and data points around the turning point are
497 under transitional regime.

498 The O₃-NO₂ relationship from the 2020s to 2060s will be mostly influenced by the
499 changing domestic anthropogenic emissions, indicated by the close distributions of data
500 points and fitted curves between “EMIS” and “2060s” in Figure 7. In the warm season,
501 the future O₃-NO₂ relations in BTH and YRD are predicted to change greatly from a
502 highly O₃ polluted situation with moderate NO₂ concentration to a situation with a
503 relatively low level of NO₂ (mostly under 10 ppb) and a moderate level of O₃ (under
504 60 ppb). A weak VOC-limited regime appeared for the whole BTH in 2020s, and there
505 is big diversity within the region, including a dense area with strong VOC-limited
506 regime and other areas with transitional or NO_x-limited regime (Figure 7a). Represented
507 by the moving of most points from the right of the turning point to near or left of the
508 turning point, the NO_x-limited and transitional regimes will dominate BTH in the 2060s.
509 Compared to 2020s, the data points of 2060s are more closely distributed, indicating a
510 reduced diversity of O₃ formation regime in the region. For YRD, most areas were
511 under transitional or weak VOC-limited regime in the 2020s with limited diversity
512 within the region, and the situation in 2060s will be similar to that of BTH (Figure 7a)



513 and 7b). The shift from weak VOC-limited regime in 2020s to transitional or NO_x-
514 limited regime in 2060s for BTH and YRD implies the influence of emission reduction
515 on altering the sensitivity of O₃ formation to precursors. Most areas of PRD in the 2020s
516 are under transitional or NO_x-limited regimes, and the regime will transfer to a strong
517 NO_x-limited one in 2060s, with an almost positive correlation between NO₂ and O₃ in
518 a low-NO₂ environment (Figure 7c). In the non-warm season, O₃ and NO₂ will remain
519 negatively correlated for BTH and YRD till the 2060s, which suggests a persistent
520 VOC-limited regime and explains the O₃ concentration growth along with substantial
521 precursor emission reductions. The turning points are simulated at extremely low NO₂
522 concentrations of 2.0 and 1.2 ppb for BTH and YRD, respectively (Figure 7d and 7e).
523 A big challenge still exists on effective emission controls to reduce the O₃ concentration
524 in the non-warm season for the two regions. Differently, the O₃ formation sensitivity in
525 most of PRD will shift from transitional regime towards a more NO_x-limited situation
526 (Figure 7f).

527 The fitted curves of other three factors are similar to those of the 2020s, and the
528 change of these factors will make little difference on NO₂ concentration but will result
529 in moderate changes on O₃ concentration within ±2 ppb. The limited changes of climate,
530 BVOCs emissions and foreign anthropogenic emissions will not essentially alter the O₃
531 formation regime, but may change the O₃ production under the nearly same NO₂
532 concentration. Changes of individual meteorological factors are expected to easily
533 influence the O₃ and NO₂ concentrations (Pope et al., 2015; Liu and Wang, 2020;
534 Dewan and Lakhani, 2022). The modeled little response of NO₂ to meteorological
535 change, except that in the non-warm season for BTH, might be attributed to the
536 compensating effect of different variables. The limited influence of BVOCs on the O₃
537 formation sensitivity to precursors is consistent with Gao et al. (2022), which reported
538 comparable empirical kinetic modelling approach (EKMA) curves with and without
539 BVOCs emissions. The transboundary O₃ pollution results from the transport of both
540 O₃ and its precursors (mainly associated with PAN), while NO₂ is less influenced by



541 long-range transport due to its shorter lifetime (Ni et al., 2018; Yin et al., 2022).

542 The change in O₃ formation regime might partly explain the finding that the joint
543 effect of multiple factors on restraining O₃ pollution will be larger than the aggregated
544 effects of individual factors. Under a NO_x-limited regime, O₃ is less sensitive to
545 changing VOCs emissions (e.g., BVOCs emissions) than that under a VOC-limited one.
546 Therefore, the enhancement of O₃ due to BVOCs emission growth in the future will be
547 restrained with a much lower NO₂ concentration. This indicates a co-benefit of reducing
548 the anthropogenic emissions to restrain the potential O₃ pollution elevation due to
549 growing BVOCs emissions (as a part of climate penalty) in the future.

550 **3.5 Change of O₃ exceedance events over the east of China**

551 Figure 8 shows the “O₃ exceedance events” over the east of China (mainly
552 including Northern, Eastern, Central and Southern China) in the 2020s and 2060s, and
553 the changes influenced by different factors. The exceedance is defined as number of
554 days with the MDA8 O₃ exceeding the Chinese National Air Quality Standard-Grade
555 II (160 μg m⁻³ or 81.6 ppb). The exceedance events appear mainly in the warm season
556 (Figure S7). Areas with frequent exceedance (over 50 days) in the 2020s were mainly
557 located in Northern China. Much fewer exceedances are found for YRD and PRD (19.3
558 and 8.2 days in 2020s, respectively). In the 2060s, the O₃ exceedance events will drop
559 significantly. The exceedance days will be fewer than 10 days for most of the country,
560 except for some areas in BTH which will still have more than 20 exceedance days over
561 the year.

562 Domestic emission abatement will be the most important factor reducing the O₃
563 exceedance, particularly in Northern China. The exceedance days will be cut by 45.3,
564 19.1 and 8.1 days for BTH, YRD and PRD, respectively, with the maximum reduction
565 reaching 80 days within BTH and YRD. Notably, the spatial pattern of changing O₃
566 exceedance due to emission reduction is different from that of changing MDA8 O₃ due
567 to emission reduction as shown in Figure 5a. Even the warm season MDA8 O₃
568 concentration of BTH will decline only 9.7 ppb, the O₃ exceedance events will be



569 greatly reduced, indicating that national emission controls will be especially effective
570 in reducing serious O₃ pollution. Climate change will mainly affect Jiangsu, Anhui,
571 Henan and Hebei provinces, elevating the exceedance by more than 15 days in most of
572 these areas. For YRD and PRD, climate change will elevate the exceedance by 9.5 and
573 3.3 days, respectively. Some areas of BTH will benefit from climate change, with the
574 exceedance declining 0–10 days. The influences of BVOCs and foreign emission
575 change on exceedance days are of limited regional differences, with a growth of 5 to 15
576 days for the former and a decline of –5 to 0 days for the latter. The exceedances elevated
577 by BVOCs emission growth will be 6.6, 6.1 and 2.8 days for BTH, YRD and PRD with
578 the maximum reaching 19, 18 and 12 days within the region, respectively, reflecting an
579 unneglectable role of biogenic source change on future O₃ episodes.

580 **4 Conclusions**

581 We explore the response of China's surface O₃ concentration to the future changes
582 of multiple factors under SSP2-45, based on a series of sensitivity experiments with
583 WRF-MEGAN-CMAQ simulations. From the 2020s to 2060s, the MDA8 O₃
584 concentration is predicted to decline by 7.7 and 1.1 ppb in the warm and non-warm
585 season, respectively, and the O₃ exceedances of Chinese National Air Quality Standard
586 (Grade II) will be largely eliminated. In the warm season, MDA8 O₃ in BTH, YRD and
587 PRD will decline by 9.7, 14.8 and 12.8 ppb, respectively, larger than the national
588 average level. However, MDA8 O₃ will increase in BTH and YRD in the non-warm
589 season attributed to the reduced NO_x emissions and thereby titration effect. The O₃
590 pollution will expand towards the non-warm season in the future, bringing new
591 challenge for policy makers to optimize the strategy of precursor emission controls
592 based on local conditions.

593 Reduction of local anthropogenic emissions is estimated to dominate the spatial
594 distribution and magnitude of future O₃ change. Meteorological variation will lead to a
595 change of MDA8 O₃ ranging between –1 and 4 ppb for most areas in the warm season.



596 The influences of changing BVOCs and foreign anthropogenic emissions will be within
597 ± 3 ppb, with the former elevating O_3 while the latter reducing O_3 . Especially in areas
598 with high O_3 pollution and intense NO_x emissions, the growing BVOCs emissions will
599 more enhance the risk of O_3 pollution. The joint effect of multiple factors on restraining
600 O_3 pollution will be larger than the aggregated effects of individual factors, which can
601 be partly explained by the changing O_3 formation regime. Large amount of emission
602 reduction under SSP2-45 will reshape the O_3 formation sensitivity to precursors. In
603 BTH and YRD, O_3 formation in the warm season is projected to shift from weak VOC-
604 limited to transitional or NO_x -limited regime, while VOC-limited regime will still
605 dominate in the non-warm season. In the future, O_3 will be less sensitive to BVOCs
606 change in a low NO_x environment along with persistent emission controls, highlighting
607 the benefit of anthropogenic emissions abatement on mitigating the climate penalty and
608 limiting O_3 pollution.

609 Limitations exist in current study. Firstly, the future climate data are taken from
610 one single model CESM, subject to bias in the assessment of meteorological influence
611 on O_3 . Secondly, some factors that will influence future O_3 level are not included in our
612 analyses, such as the changing CH_4 concentration and the stratosphere-troposphere
613 exchange of O_3 . Thirdly, there exist gaps between the downscaled and realistic
614 conditions of meteorology for the 2020s, leading to uncertainty in the O_3 simulation.
615 Finally, the changing O_3 formation regime is presented through the relation between O_3
616 and NO_2 concentrations, and the mechanism how the climate penalty will influence O_3
617 formation under substantial reduction of anthropogenic emissions needs to be better
618 analyzed in future studies.

619 **Data availability**

620 All data in this study are available from the authors upon request.

621 **Author contributions**

622 JYang developed the methodology, conducted the work and wrote the draft. YZhao



623 improved the methodology, supervised the work and revised the manuscript. YWang
624 and LZhang contributed to the methodology and provided supports to the scientific
625 interpretation and discussions.

626 **Competing interests**

627 The authors declare that they have no conflict of interest.

628 **Acknowledgments**

629 This work was sponsored by the National Key Research and Development
630 Program of China (2023YFC3709802), National Natural Science Foundation of China
631 (42177080), and the Key Research and Development Programme of Jiangsu Province
632 (BE2022838). We thank Qiang Zhang and Dan Tong from Tsinghua University for the
633 emission data (MEIC and DPEC).



634 **References**

- 635 Akimoto, H. and Tanimoto, H.: Rethinking of the adverse effects of NO_x-control on the
636 reduction of methane and tropospheric ozone – Challenges toward a denitrified society,
637 *Atmos. Environ.*, 277, 119033, [10.1016/j.atmosenv.2022.119033](https://doi.org/10.1016/j.atmosenv.2022.119033), 2022.
- 638 Andersson, C. and Engardt, M.: European ozone in a future climate: Importance of
639 changes in dry deposition and isoprene emissions, *J. Geophys. Res.-Atmos.*, 115,
640 D02303, [10.1029/2008jd011690](https://doi.org/10.1029/2008jd011690), 2010.
- 641 Appel, K. W., Pouliot, G. A., Simon, H., Sarwar, G., Pye, H. O. T., Napelenok, S. L.,
642 Akhtar, F., and Roselle, S. J.: Evaluation of dust and trace metal estimates from the
643 Community Multiscale Air Quality (CMAQ) model version 5.0, *Geosci. Model Dev.*,
644 6, 883–899, [10.5194/gmd-6-883-2013](https://doi.org/10.5194/gmd-6-883-2013), 2013.
- 645 Avnery, S., Mauzerall, D. L., Liu, J., and Horowitz, L. W.: Global crop yield reductions
646 due to surface ozone exposure: 1. Year 2000 crop production losses and economic
647 damage, *Atmos. Environ.*, 45, 2284–2296, [10.1016/j.atmosenv.2010.11.045](https://doi.org/10.1016/j.atmosenv.2010.11.045), 2011.
- 648 Cao, J., Situ, S., Hao, Y., Xie, S., and Li, L.: Enhanced summertime ozone and SOA
649 from biogenic volatile organic compound (BVOC) emissions due to vegetation biomass
650 variability during 1981–2018 in China, *Atmos. Chem. Phys.*, 22, 2351–2364,
651 [10.5194/acp-22-2351-2022](https://doi.org/10.5194/acp-22-2351-2022), 2022.
- 652 Chen, J., Avise, J., Guenther, A., Wiedinmyer, C., Salathe, E., Jackson, R. B., and Lamb,
653 B.: Future land use and land cover influences on regional biogenic emissions and air
654 quality in the United States, *Atmos. Environ.*, 43, 5771–5780,
655 [10.1016/j.atmosenv.2009.08.015](https://doi.org/10.1016/j.atmosenv.2009.08.015), 2009.
- 656 Chen, X., Jiang, Z., Shen, Y., Li, R., Fu, Y., Liu, J., Han, H., Liao, H., Cheng, X., Jones,
657 D. B. A., Worden, H., and Abad, G. G.: Chinese Regulations Are Working—Why Is
658 Surface Ozone Over Industrialized Areas Still High? Applying Lessons From Northeast
659 US Air Quality Evolution, *Geophys. Res. Lett.*, 48, e2021GL092816,



- 660 10.1029/2021gl092816, 2021.
- 661 Cheng, J., Tong, D., Liu, Y., Yu, S., Yan, L., Zheng, B., Geng, G., He, K., and Zhang,
662 Q.: Comparison of Current and Future PM_{2.5} Air Quality in China Under CMIP6 and
663 DPEC Emission Scenarios, *Geophys. Res. Lett.*, 48, e2021GL093197,
664 10.1029/2021gl093197, 2021a.
- 665 Cheng, J., Tong, D., Zhang, Q., Liu, Y., Lei, Y., Yan, G., Yan, L., Yu, S., Cui, R. Y.,
666 Clarke, L., Geng, G., Zheng, B., Zhang, X., Davis, S. J., and He, K.: Pathways of
667 China's PM_{2.5} air quality 2015–2060 in the context of carbon neutrality, *Natl. Sci. Rev.*,
668 8, nwab078, 10.1093/nsr/nwab078, 2021b.
- 669 Dewan, S. and Lakhani, A.: Tropospheric ozone and its natural precursors impacted by
670 climatic changes in emission and dynamics, *Front. Environ. Sci.*, 10, 1007942,
671 10.3389/fenvs.2022.1007942, 2022.
- 672 Feng, Y., Ning, M., Xue, W., Cheng, M., and Lei, Y.: Developing China's roadmap for
673 air quality improvement: A review on technology development and future prospects, *J.*
674 *Environ. Sci.*, 123, 510–521, 10.1016/j.jes.2022.10.028, 2023.
- 675 Feng, Z. Z., Xu, Y. S., Kobayashi, K., Dai, L. L., Zhang, T. Y., Agathokleous, E.,
676 Calatayud, V., Paoletti, E., Mukherjee, A., Agrawal, M., Park, R. J., Oak, Y. J., and
677 Yue, X.: Ozone pollution threatens the production of major staple crops in East Asia,
678 *Nat. Food*, 3, 47–56, 10.1038/s43016-021-00422-6, 2022.
- 679 FinlaysonPitts, B. J. and Pitts, J. N.: Tropospheric air pollution: Ozone, airborne toxics,
680 polycyclic aromatic hydrocarbons, and particles, *Science*, 276, 1045–1052,
681 10.1126/science.276.5315.1045, 1997.
- 682 Fischer, E. V., Jacob, D. J., Yantosca, R. M., Sulprizio, M. P., Millet, D. B., Mao, J.,
683 Paulot, F., Singh, H. B., Roiger, A., Ries, L., Talbot, R. W., Dzepina, K., and Pandey
684 Deolal, S.: Atmospheric peroxyacetyl nitrate (PAN): a global budget and source
685 attribution, *Atmos. Chem. Phys.*, 14, 2679–2698, 10.5194/acp-14-2679-2014, 2014.



- 686 Gao, M., Gao, J., Zhu, B., Kumar, R., Lu, X., Song, S., Zhang, Y., Jia, B., Wang, P.,
687 Beig, G., Hu, J., Ying, Q., Zhang, H., Sherman, P., and McElroy, M. B.: Ozone
688 pollution over China and India: seasonality and sources, *Atmos. Chem. Phys.*, 20,
689 4399–4414, 10.5194/acp-20-4399-2020, 2020.
- 690 Gao, M., Wang, F., Ding, Y., Wu, Z., Xu, Y., Lu, X., Wang, Z., Carmichael, G. R., and
691 McElroy, M. B.: Large-scale climate patterns offer preseasonal hints on the co-
692 occurrence of heat wave and O₃ pollution in China, *Proc. Natl. Acad. Sci. U.S.A.*, 120,
693 e2218274120, 10.1073/pnas.2218274120, 2023.
- 694 Gao, Y., Fu, J. S., Drake, J. B., Lamarque, J. F., and Liu, Y.: The impact of emission
695 and climate change on ozone in the United States under representative concentration
696 pathways (RCPs), *Atmos. Chem. Phys.*, 13, 9607–9621, 10.5194/acp-13-9607-2013,
697 2013.
- 698 Gao, Y., Yan, F., Ma, M., Ding, A., Liao, H., Wang, S., Wang, X., Zhao, B., Cai, W.,
699 Su, H., Yao, X., and Gao, H.: Unveiling the dipole synergic effect of biogenic and
700 anthropogenic emissions on ozone concentrations, *Sci. Total. Env.*, 818, 151722,
701 10.1016/j.scitotenv.2021.151722, 2022.
- 702 Gidden, M. J., Riahi, K., Smith, S. J., Fujimori, S., Luderer, G., Kriegler, E., van Vuuren,
703 D. P., van den Berg, M., Feng, L., Klein, D., Calvin, K., Doelman, J. C., Frank, S.,
704 Fricko, O., Harmsen, M., Hasegawa, T., Havlik, P., Hilaire, J., Hoesly, R., Horing, J.,
705 Popp, A., Stehfest, E., and Takahashi, K.: Global emissions pathways under different
706 socioeconomic scenarios for use in CMIP6: a dataset of harmonized emissions
707 trajectories through the end of the century, *Geosci. Model Dev.*, 12, 1443–1475,
708 10.5194/gmd-12-1443-2019, 2019.
- 709 Gong, C. and Liao, H.: A typical weather pattern for ozone pollution events in North
710 China, *Atmos. Chem. Phys.*, 19, 13725–13740, 10.5194/acp-19-13725-2019, 2019.
- 711 Gonzalez-Abraham, R., Chung, S. H., Avise, J., Lamb, B., Salathe, E. P., Jr., Nolte, C.



- 712 G., Loughlin, D., Guenther, A., Wiedinmyer, C., Duhl, T., Zhang, Y., and Streets, D.
713 G.: The effects of global change upon United States air quality, *Atmos. Chem. Phys.*,
714 15, 12645–12665, 10.5194/acp-15-12645-2015, 2015.
- 715 Guenther, A. B., Jiang, X., Heald, C. L., Sakulyanontvittaya, T., Duhl, T., Emmons, L.
716 K., and Wang, X.: The Model of Emissions of Gases and Aerosols from Nature version
717 2.1 (MEGAN2.1): an extended and updated framework for modeling biogenic
718 emissions, *Geosci. Model Dev.*, 5, 1471–1492, 10.5194/gmd-5-1471-2012, 2012.
- 719 Han, H., Liu, J., Yuan, H., Wang, T., Zhuang, B., and Zhang, X.: Foreign influences on
720 tropospheric ozone over East Asia through global atmospheric transport, *Atmos. Chem.*
721 *Phys.*, 19, 12495–12514, 10.5194/acp-19-12495-2019, 2019.
- 722 Han, H., Liu, J., Shu, L., Wang, T., and Yuan, H.: Local and synoptic meteorological
723 influences on daily variability in summertime surface ozone in eastern China, *Atmos.*
724 *Chem. Phys.*, 20, 203–222, 10.5194/acp-20-203-2020, 2020.
- 725 Harper, K. L. and Unger, N.: Global climate forcing driven by altered BVOC fluxes
726 from 1990 to 2010 land cover change in maritime Southeast Asia, *Atmos. Chem. Phys.*,
727 18, 16931–16952, 10.5194/acp-18-16931-2018, 2018.
- 728 Hollaway, M. J., Arnold, S. R., Collins, W. J., Folberth, G., and Rap, A.: Sensitivity of
729 midnineteenth century tropospheric ozone to atmospheric chemistry-vegetation
730 interactions, *J. Geophys. Res.-Atmos.*, 122, 2452–2473, 10.1002/2016jd025462, 2017.
- 731 Hong, C., Zhang, Q., Zhang, Y., Davis, S. J., Tong, D., Zheng, Y., Liu, Z., Guan, D.,
732 He, K., and Schellnhuber, H. J.: Impacts of climate change on future air quality and
733 human health in China, *Proc. Natl. Acad. Sci. U.S.A.*, 116, 17193–17200,
734 10.1073/pnas.1812881116, 2019.
- 735 Hu, A., Xie, X., Gong, K., Hou, Y., Zhao, Z., and Hu, J.: Assessing the Impacts of
736 Climate Change on Meteorology and Air Stagnation in China Using a Dynamical
737 Downscaling Method, *Front. Environ. Sci.*, 10, 894887, 10.3389/fenvs.2022.894887,



- 738 2022.
- 739 Hu, J., Chen, J., Ying, Q., and Zhang, H.: One-year simulation of ozone and particulate
740 matter in China using WRF/CMAQ modeling system, *Atmos. Chem. Phys.*, 16, 10333–
741 10350, 10.5194/acp-16-10333-2016, 2016.
- 742 Hurtt, G. C., Chini, L., Sahajpal, R., Frolking, S., Boudirsky, B. L., Calvin, K., Doelman,
743 J. C., Fisk, J., Fujimori, S., Klein Goldewijk, K., Hasegawa, T., Havlik, P., Heinemann,
744 A., Humpenöder, F., Jungclaus, J., Kaplan, J. O., Kennedy, J., Krisztin, T., Lawrence,
745 D., Lawrence, P., Ma, L., Mertz, O., Pongratz, J., Popp, A., Poulter, B., Riahi, K.,
746 Shevliakova, E., Stehfest, E., Thornton, P., Tubiello, F. N., van Vuuren, D. P., and
747 Zhang, X.: Harmonization of global land use change and management for the period
748 850–2100 (LUH2) for CMIP6, *Geosci. Model Dev.*, 13, 5425–5464, 10.5194/gmd-13-
749 5425-2020, 2020.
- 750 IPCC: Climate Change 2021 – The Physical Science Basis: Working Group I
751 Contribution to the Sixth Assessment Report of the Intergovernmental Panel on Climate
752 Change, Cambridge University Press, Cambridge, 10.1017/9781009157896, 2021.
- 753 IPCC: Climate Change 2022: Mitigation of Climate Change: Working Group III
754 Contribution to the Sixth Assessment Report of the Intergovernmental Panel on Climate
755 Change, Cambridge University Press, Cambridge, 10.1017/9781009157926, 2022.
- 756 Jerrett, M., Burnett, R. T., Pope, C. A., 3rd, Ito, K., Thurston, G., Krewski, D., Shi, Y.,
757 Calle, E., and Thun, M.: Long-term ozone exposure and mortality, *N. Engl. J. Med.*,
758 360, 1085–1095, 10.1056/NEJMoa0803894, 2009.
- 759 Jiang, Y., Ding, D., Dong, Z., Liu, S., Chang, X., Zheng, H., Xing, J., and Wang, S.:
760 Extreme Emission Reduction Requirements for China to Achieve World Health
761 Organization Global Air Quality Guidelines, *Environ. Sci. Technol.*, 57, 4424–4433,
762 10.1021/acs.est.2c09164, 2023.
- 763 Jin, X. and Holloway, T.: Spatial and temporal variability of ozone sensitivity over



- 764 China observed from the Ozone Monitoring Instrument, *J. Geophys. Res.-Atmos.*, 120,
765 7229–7246, 10.1002/2015jd023250, 2015.
- 766 Li, H., Yang, Y., Jin, J., Wang, H., Li, K., Wang, P., and Liao, H.: Climate-driven
767 deterioration of future ozone pollution in Asia predicted by machine learning with
768 multi-source data, *Atmos. Chem. Phys.*, 23, 1131–1145, 10.5194/acp-23-1131-2023,
769 2023.
- 770 Li, K., Jacob, D. J., Shen, L., Lu, X., De Smedt, I., and Liao, H.: Increases in surface
771 ozone pollution in China from 2013 to 2019: anthropogenic and meteorological
772 influences, *Atmos. Chem. Phys.*, 20, 11423–11433, 10.5194/acp-20-11423-2020,
773 2020a.
- 774 Li, K., Jacob, D. J., Liao, H., Qiu, Y., Shen, L., Zhai, S., Bates, K. H., Sulprizio, M. P.,
775 Song, S., Lu, X., Zhang, Q., Zheng, B., Zhang, Y., Zhang, J., Lee, H. C., and Kuk, S.
776 K.: Ozone pollution in the North China Plain spreading into the late-winter haze season,
777 *Proc. Natl. Acad. Sci. U.S.A.*, 118, e2015797118, 10.1073/pnas.2015797118, 2021.
- 778 Li, L., Yang, W., Xie, S., and Wu, Y.: Estimations and uncertainty of biogenic volatile
779 organic compound emission inventory in China for 2008-2018, *Sci. Total. Env.*, 733,
780 139301, 10.1016/j.scitotenv.2020.139301, 2020b.
- 781 Li, M., Zhang, Q., Kurokawa, J.-i., Woo, J.-H., He, K., Lu, Z., Ohara, T., Song, Y.,
782 Streets, D. G., Carmichael, G. R., Cheng, Y., Hong, C., Huo, H., Jiang, X., Kang, S.,
783 Liu, F., Su, H., and Zheng, B.: MIX: a mosaic Asian anthropogenic emission inventory
784 under the international collaboration framework of the MICS-Asia and HTAP, *Atmos.*
785 *Chem. Phys.*, 17, 935–963, 10.5194/acp-17-935-2017, 2017.
- 786 Liang, S., Cheng, J., Jia, K., Jiang, B., Liu, Q., Xiao, Z., Yao, Y., Yuan, W., Zhang, X.,
787 Zhao, X., and Zhou, J.: The Global Land Surface Satellite (GLASS) Product Suite, *Bull.*
788 *Am. Meteorol. Soc.*, 102, E323–E337, 10.1175/bams-d-18-0341.1, 2021.
- 789 Liao, W., Liu, X., Xu, X., Chen, G., Liang, X., Zhang, H., and Li, X.: Projections of



- 790 land use changes under the plant functional type classification in different SSP-RCP
791 scenarios in China, *Sci. Bull.*, 65, 1935–1947, 10.1016/j.scib.2020.07.014, 2020.
- 792 Liu, Q., Lam, K. S., Jiang, F., Wang, T. J., Xie, M., Zhuang, B. L., and Jiang, X. Y.: A
793 numerical study of the impact of climate and emission changes on surface ozone over
794 South China in autumn time in 2000–2050, *Atmos. Environ.*, 76, 227–237,
795 10.1016/j.atmosenv.2013.01.030, 2013.
- 796 Liu, S., Xing, J., Zhang, H., Ding, D., Zhang, F., Zhao, B., Sahu, S. K., and Wang, S.:
797 Climate-driven trends of biogenic volatile organic compound emissions and their
798 impacts on summertime ozone and secondary organic aerosol in China in the 2050s,
799 *Atmos. Environ.*, 218, 117020, 10.1016/j.atmosenv.2019.117020, 2019.
- 800 Liu, S., Sahu, S. K., Zhang, S., Liu, S., Sun, Y., Liu, X., Xing, J., Zhao, B., Zhang, H.,
801 and Wang, S.: Impact of Climate-Driven Land-Use Change on O₃ and PM Pollution by
802 Driving BVOC Emissions in China in 2050, *Atmosphere*, 13, 1086,
803 10.3390/atmos13071086, 2022.
- 804 Liu, Y. and Wang, T.: Worsening urban ozone pollution in China from 2013 to 2017-
805 Part 1: The complex and varying roles of meteorology, *Atmos. Chem. Phys.*, 20, 6305–
806 6321, 10.5194/acp-20-6305-2020, 2020.
- 807 Liu, Y., Geng, G., Cheng, J., Liu, Y., Xiao, Q., Liu, L., Shi, Q., Tong, D., He, K., and
808 Zhang, Q.: Drivers of Increasing Ozone during the Two Phases of Clean Air Actions in
809 China 2013–2020, *Environ. Sci. Technol.*, 57, 8954–8964, 10.1021/acs.est.3c00054,
810 2023.
- 811 Lu, X., Zhang, L., and Shen, L.: Meteorology and Climate Influences on Tropospheric
812 Ozone: a Review of Natural Sources, Chemistry, and Transport Patterns, *Curr. Pollut.*
813 *Rep.*, 5, 238–260, 10.1007/s40726-019-00118-3, 2019.
- 814 Meinshausen, M., Nicholls, Z. R. J., Lewis, J., Gidden, M. J., Vogel, E., Freund, M.,
815 Beyerle, U., Gessner, C., Nauels, A., Bauer, N., Canadell, J. G., Daniel, J. S., John, A.,



- 816 Krummel, P. B., Luderer, G., Meinshausen, N., Montzka, S. A., Rayner, P. J., Reimann,
817 S., Smith, S. J., van den Berg, M., Velders, G. J. M., Vollmer, M. K., and Wang, R. H.
818 J.: The shared socio-economic pathway (SSP) greenhouse gas concentrations and their
819 extensions to 2500, *Geosci. Model Dev.*, 13, 3571–3605, 10.5194/gmd-13-3571-2020,
820 2020.
- 821 Monaghan, A. J., Steinhoff, D. F., Bruyere, C. L., and Yates, D.: NCAR CESM Global
822 Bias-Corrected CMIP5 Output to Support WRF/MPAS Research, Research Data
823 Archive at the National Center for Atmospheric Research, Computational and
824 Information Systems Laboratory [dataset], 10.5065/D6DJ5CN4, 2014.
- 825 Monks, P. S., Archibald, A. T., Colette, A., Cooper, O., Coyle, M., Derwent, R., Fowler,
826 D., Granier, C., Law, K. S., Mills, G. E., Stevenson, D. S., Tarasova, O., Thouret, V.,
827 von Schneidemesser, E., Sommariva, R., Wild, O., and Williams, M. L.: Tropospheric
828 ozone and its precursors from the urban to the global scale from air quality to short-
829 lived climate forcer, *Atmos. Chem. Phys.*, 15, 8889–8973, 10.5194/acp-15-8889-2015,
830 2015.
- 831 Ni, R., Lin, J., Yan, Y., and Lin, W.: Foreign and domestic contributions to springtime
832 ozone over China, *Atmos. Chem. Phys.*, 18, 11447–11469, 10.5194/acp-18-11447-
833 2018, 2018.
- 834 O'Neill, B. C., Tebaldi, C., van Vuuren, D. P., Eyring, V., Friedlingstein, P., Hurtt, G.,
835 Knutti, R., Kriegler, E., Lamarque, J.-F., Lowe, J., Meehl, G. A., Moss, R., Riahi, K.,
836 and Sanderson, B. M.: The Scenario Model Intercomparison Project (ScenarioMIP) for
837 CMIP6, *Geosci. Model Dev.*, 9, 3461–3482, 10.5194/gmd-9-3461-2016, 2016.
- 838 Penuelas, J. and Llusia, J.: BVOCs: plant defense against climate warming?, *Trends*
839 *Plant Sci.*, 8, 105–109, 10.1016/s1360-1385(03)00008-6, 2003.
- 840 Penuelas, J. and Staudt, M.: BVOCs and global change, *Trends Plant Sci.*, 15, 133–144,
841 10.1016/j.tplants.2009.12.005, 2010.



- 842 Pope, R. J., Savage, N. H., Chipperfield, M. P., Ordóñez, C., and Neal, L. S.: The
843 influence of synoptic weather regimes on UK air quality: regional model studies of
844 tropospheric column NO₂, *Atmos. Chem. Phys.*, 15, 11201–11215, 10.5194/acp-15-
845 11201-2015, 2015.
- 846 Porter, W. C. and Heald, C. L.: The mechanisms and meteorological drivers of the
847 summertime ozone–temperature relationship, *Atmos. Chem. Phys.*, 19, 13367–13381,
848 10.5194/acp-19-13367-2019, 2019.
- 849 Riahi, K., van Vuuren, D. P., Kriegler, E., Edmonds, J., O’Neill, B. C., Fujimori, S.,
850 Bauer, N., Calvin, K., Dellink, R., Fricko, O., Lutz, W., Popp, A., Cuaresma, J. C., Kc,
851 S., Leimbach, M., Jiang, L., Kram, T., Rao, S., Emmerling, J., Ebi, K., Hasegawa, T.,
852 Havlik, P., Humpenöder, F., Da Silva, L. A., Smith, S., Stehfest, E., Bosetti, V., Eom,
853 J., Gernaat, D., Masui, T., Rogelj, J., Strefler, J., Drouet, L., Krey, V., Luderer, G.,
854 Harmsen, M., Takahashi, K., Baumstark, L., Doelman, J. C., Kainuma, M., Klimont,
855 Z., Marangoni, G., Lotze-Campen, H., Obersteiner, M., Tabeau, A., and Tavoni, M.:
856 The Shared Socioeconomic Pathways and their energy, land use, and greenhouse gas
857 emissions implications: An overview, *Glob. Environ. Change*, 42, 153–168,
858 10.1016/j.gloenvcha.2016.05.009, 2017.
- 859 Schroeder, J. R., Crawford, J. H., Fried, A., Walega, J., Weinheimer, A., Wisthaler, A.,
860 Müller, M., Mikoviny, T., Chen, G., Shook, M., Blake, D. R., and Tonnesen, G. S.:
861 New insights into the column CH₂O/NO₂ ratio as an indicator of near-surface ozone
862 sensitivity, *J. Geophys. Res.-Atmos.*, 122, 8885–8907, 10.1002/2017jd026781, 2017.
- 863 Shi, X., Zheng, Y., Lei, Y., Xue, W., Yan, G., Liu, X., Cai, B., Tong, D., and Wang, J.:
864 Air quality benefits of achieving carbon neutrality in China, *Sci. Total. Env.*, 795,
865 148784, 10.1016/j.scitotenv.2021.148784, 2021.
- 866 Sillman, S. and He, D.: Some theoretical results concerning O₃-NO_x-VOC chemistry
867 and NO_x-VOC indicators, *J. Geophys. Res.-Atmos.*, 107, 4659, 10.1029/2001jd001123,
868 2002.



- 869 Sheffield, J. and Wood, E. F.: Projected changes in drought occurrence under future
870 global warming from multi-model, multi-scenario, IPCC AR4 simulations, *Clim. Dyn.*,
871 31, 79–105, 10.1007/s00382-007-0340-z, 2008.
- 872 Szogs, S., Arneth, A., Anthoni, P., Doelman, J. C., Humpenöder, F., Popp, A., Pugh, T.
873 A. M., and Stehfest, E.: Impact of LULCC on the emission of BVOCs during the 21st
874 century, *Atmos. Environ.*, 165, 73–87, 10.1016/j.atmosenv.2017.06.025, 2017.
- 875 Tai, A. P. K. and Val Martin, M.: Impacts of ozone air pollution and temperature
876 extremes on crop yields: Spatial variability, adaptation and implications for future food
877 security, *Atmos. Environ.*, 169, 11–21, 10.1016/j.atmosenv.2017.09.002, 2017.
- 878 Tong, D., Cheng, J., Liu, Y., Yu, S., Yan, L., Hong, C. P., Qin, Y., Zhao, H. Y., Zheng,
879 Y. X., Geng, G. N., Li, M., Liu, F., Zhang, Y. X., Zheng, B., Clarke, L., and Zhang, Q.:
880 Dynamic projection of anthropogenic emissions in China: methodology and 2015-2050
881 emission pathways under a range of socio-economic, climate policy, and pollution
882 control scenarios, *Atmos. Chem. Phys.*, 20, 5729–5757, 10.5194/acp-20-5729-2020,
883 2020.
- 884 van Vuuren, D. P., Edmonds, J., Kainuma, M., Riahi, K., Thomson, A., Hibbard, K.,
885 Hurtt, G. C., Kram, T., Krey, V., Lamarque, J. F., Masui, T., Meinshausen, M.,
886 Nakicenovic, N., Smith, S. J., and Rose, S. K.: The representative concentration
887 pathways: an overview, *Clim. Change*, 109, 5–31, 10.1007/s10584-011-0148-z, 2011.
- 888 von Schneidmesser, E., Monks, P. S., Allan, J. D., Bruhwiler, L., Forster, P., Fowler,
889 D., Lauer, A., Morgan, W. T., Paasonen, P., Righi, M., Sindelarova, K., and Sutton, M.
890 A.: Chemistry and the Linkages between Air Quality and Climate Change, *Chem. Rev.*,
891 115, 3856–3897, 10.1021/acs.chemrev.5b00089, 2015.
- 892 Wang, H., Wu, Q., Guenther, A. B., Yang, X., Wang, L., Xiao, T., Li, J., Feng, J., Xu,
893 Q., and Cheng, H.: A long-term estimation of biogenic volatile organic compound
894 (BVOC) emission in China from 2001–2016: the roles of land cover change and climate



- 895 variability, *Atmos. Chem. Phys.*, 21, 4825–4848, 10.5194/acp-21-4825-2021, 2021a.
- 896 Wang, L., Tai, A. P. K., Tam, C.-Y., Sadiq, M., Wang, P., and Cheung, K. K. W.:
897 Impacts of future land use and land cover change on mid-21st-century surface ozone
898 air quality: distinguishing between the biogeophysical and biogeochemical effects,
899 *Atmos. Chem. Phys.*, 20, 11349–11369, 10.5194/acp-20-11349-2020, 2020.
- 900 Wang, N., Xu, J., Pei, C., Tang, R., Zhou, D., Chen, Y., Li, M., Deng, X., Deng, T.,
901 Huang, X., and Ding, A.: Air Quality During COVID-19 Lockdown in the Yangtze
902 River Delta and the Pearl River Delta: Two Different Responsive Mechanisms to
903 Emission Reductions in China, *Environ. Sci. Technol.*, 55, 5721–5730,
904 10.1021/acs.est.0c08383, 2021b.
- 905 Wang, P., Yang, Y., Li, H., Chen, L., Dang, R., Xue, D., Li, B., Tang, J., Leung, L. R.,
906 and Liao, H.: North China Plain as a hot spot of ozone pollution exacerbated by extreme
907 high temperatures, *Atmos. Chem. Phys.*, 22, 4705–4719, 10.5194/acp-22-4705-2022,
908 2022.
- 909 Wang, Y., Zhao, Y., Liu, Y., Jiang, Y., Zheng, B., Xing, J., Liu, Y., Wang, S., and
910 Nielsen, C. P.: Sustained emission reductions have restrained the ozone pollution over
911 China, *Nat. Geosci.*, 10.1038/s41561-023-01284-2, 2023.
- 912 Weng, X., Forster, G. L., and Nowack, P.: A machine learning approach to quantify
913 meteorological drivers of ozone pollution in China from 2015 to 2019, *Atmos. Chem.*
914 *Phys.*, 22, 8385–8402, 10.5194/acp-22-8385-2022, 2022.
- 915 Wu, K., Yang, X., Chen, D., Gu, S., Lu, Y., Jiang, Q., Wang, K., Ou, Y., Qian, Y., Shao,
916 P., and Lu, S.: Estimation of biogenic VOC emissions and their corresponding impact
917 on ozone and secondary organic aerosol formation in China, *Atmos. Res.*, 231, 104656,
918 10.1016/j.atmosres.2019.104656, 2020.
- 919 Xiao, Q., Geng, G., Xue, T., Liu, S., Cai, C., He, K., and Zhang, Q.: Tracking PM_{2.5}
920 and O₃ Pollution and the Related Health Burden in China 2013–2020, *Environ. Sci.*



- 921 Technol., 56, 6922–6932, 10.1021/acs.est.1c04548, 2022.
- 922 Xu, B., Wang, T., Ma, D., Song, R., Zhang, M., Gao, L., Li, S., Zhuang, B., Li, M., and
923 Xie, M.: Impacts of regional emission reduction and global climate change on air
924 quality and temperature to attain carbon neutrality in China, *Atmos. Res.*, 279, 106384,
925 10.1016/j.atmosres.2022.106384, 2022.
- 926 Yang, J. and Zhao, Y.: Performance and application of air quality models on ozone
927 simulation in China – A review, *Atmos. Environ.*, 293, 119446,
928 10.1016/j.atmosenv.2022.119446, 2023.
- 929 Yarwood, G., Rao, S., Yocke, M., and Whitten, G.: Updates to the Carbon Bond
930 Mechanism: CB05, Yocke and Company Final Rep. to the U.S, 2005.
- 931 Yin, H., Sun, Y., Notholt, J., Palm, M., and Liu, C.: Spaceborne tropospheric nitrogen
932 dioxide (NO₂) observations from 2005–2020 over the Yangtze River Delta (YRD),
933 China: variabilities, implications, and drivers, *Atmos. Chem. Phys.*, 22, 4167–4185,
934 10.5194/acp-22-4167-2022, 2022.
- 935 Zheng, B., Tong, D., Li, M., Liu, F., Hong, C. P., Geng, G. N., Li, H. Y., Li, X., Peng,
936 L. Q., Qi, J., Yan, L., Zhang, Y. X., Zhao, H. Y., Zheng, Y. X., He, K. B., and Zhang,
937 Q.: Trends in China's anthropogenic emissions since 2010 as the consequence of clean
938 air actions, *Atmos. Chem. Phys.*, 18, 14095–14111, 10.5194/acp-18-14095-2018, 2018.
- 939 Zhu, J. and Liao, H.: Future ozone air quality and radiative forcing over China owing
940 to future changes in emissions under the Representative Concentration Pathways
941 (RCPs), *J. Geophys. Res.-Atmos.*, 121, 1978–2001, 10.1002/2015jd023926, 2016.
- 942 Zhu, J., Tai, A. P. K., and Hung Lam Yim, S.: Effects of ozone–vegetation interactions
943 on meteorology and air quality in China using a two-way coupled land–atmosphere
944 model, *Atmos. Chem. Phys.*, 22, 765–782, 10.5194/acp-22-765-2022, 2022.
- 945



946 **FIGURE CAPTIONS**

947 Figure 1 The modelling domain and geographical definitions (denoted by colors) of this
948 study. Boundaries of the three regions, including BTH (Beijing-Tianjin-Hebei), YRD
949 (Yangtze River Delta) and PRD (Pearl River Delta), are marked by dark grey lines.

950 Figure 2 Projected changes of the strongly ozone-related meteorological elements, daily
951 maximum temperature at 2 m (T-max, a and d), relative humidity (RH, b and e) and
952 wind speed (WS, c and f), from the 2020s to 2060s. Panels (a-c) represent those of the
953 warm season, and panels (d-f) represent those of non-warm season.

954 Figure 3 Simulation and projection of seasonal average MDA8 O₃ in the 2020s (Case1,
955 a and b) and 2060s (Case2, d and e), and the changes over this period (Case2–Case1, c
956 and f). Panels (a-c) represent those of the warm season, and panels (d-f) represent those
957 of non-warm season. Regional mean concentrations across China (CHN), BTH, YRD
958 and PRD are inset.

959 Figure 4 Simulation and projection of monthly average MDA8 O₃ in the 2020s and
960 2060s across CHN (a), BTH (b), YRD (c) and PRD (d).

961 Figure 5 Projected changes of MDA8 O₃ from the 2020s to 2060s attributed to
962 anthropogenic emissions from local sources (Case3–Case1, a and e), meteorological
963 conditions (Case4–Case1, b and f), BVOCs emissions (Case5–Case1, c and g) and
964 anthropogenic emissions from surrounding countries (Case6–Case1, d and h). Panels
965 (a-d) represent those of the warm season, and panels (e-h) represent those of non-warm
966 season. Regional mean changes across CHN, BTH, YRD and PRD are inset.

967 Figure 6 The relationships between the separate MDA8 O₃ changes attributed to the
968 four factors (denoted by the name of Case3–6) and the total changes from the 2020s to
969 2060s over China and the three regions. Panels (a-d) represent those of the warm season,
970 and panels (e-h) represent those of non-warm season. The relative contributions of the



971 four factors to the total influence of future change are shown in the light grey box.

972 Figure 7 The relationships between simulated hourly NO_2 and O_3 concentrations with
973 the lognormal fits for different regions and seasons. The colored circles, representing
974 different cases, come from the seasonal average concentrations for each grid in the
975 target region. The specific circles with black border represent the regional average
976 situation, and the turning points of every fitted curve are marked by the “+” sign. The
977 density plots of the 2020s and 2060s are inset.

978 Figure 8 Projected annual O_3 exceedance over the east of China in the 2020s and 2060s,
979 and the exceedance changes when the four factors at 2060s level. Regional mean
980 changes across CHN, BTH, YRD and PRD are inset.

981



982 **TABLES**

983 **Table 1. List of simulation cases to investigate the impact of future change upon**
984 **surface O₃ in China, with sensitivity experiments from the perspectives of four**
985 **main influencing factors.**

Case number	Case name	China's local emissions	Meteorological conditions	BVOCs emissions	Surrounding emissions
Case1	2020s	2020	2018-2022	2018-2022	2020
Case2	2060s	2060	2058-2062	2058-2062	2060
Case3	EMIS	2060	2018-2022	2018-2022	2020
Case4	CLIM	2020	2058-2062	2018-2022	2020
Case5	BVOC	2020	2018-2022	2058-2062	2020
Case6	SURR	2020	2018-2022	2018-2022	2060

986

987

988 **Table 2. The BVOCs estimation over China and emission intensity in BTH, YRD**
989 **and PRD of the 2020s and 2060s, as well as the corresponding growth rates over**
990 **this period.**

	China	BTH	YRD	PRD
	Emissions (Tg)	Emission intensity (Gg grid ⁻¹)		
2020s	33.6	1.4	4.6	8.7
2060s	43.4	1.7	5.7	10.7
Growth rate	29.2 %	21.4 %	23.9 %	23.0 %

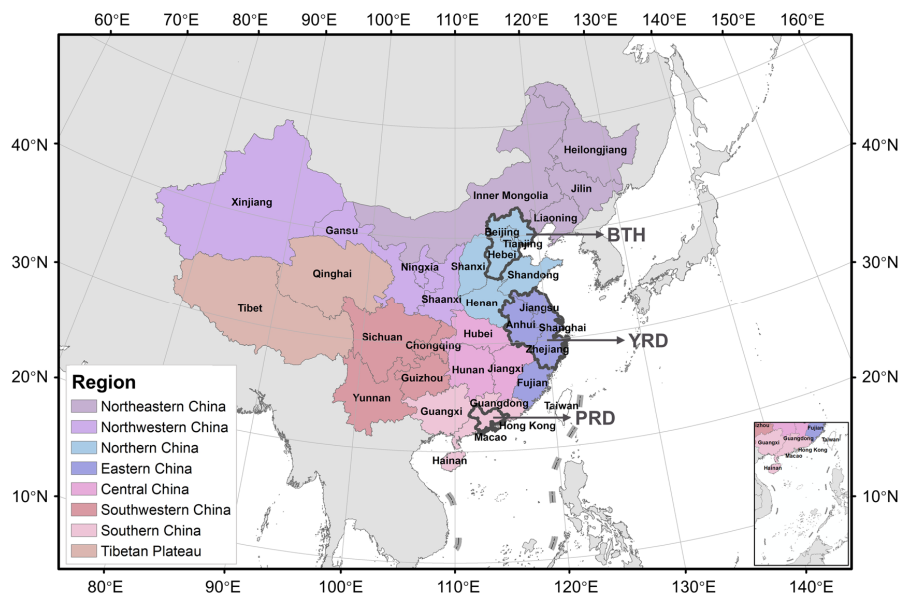
991

992



993 **FIGURES**

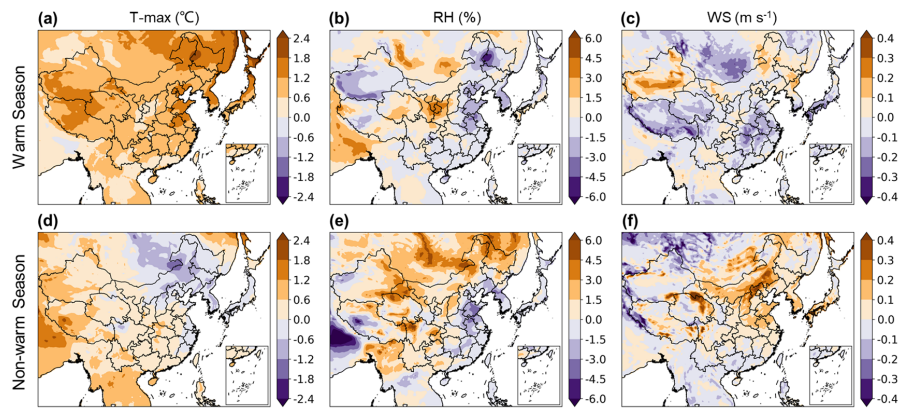
994 **Figure 1**



995
996



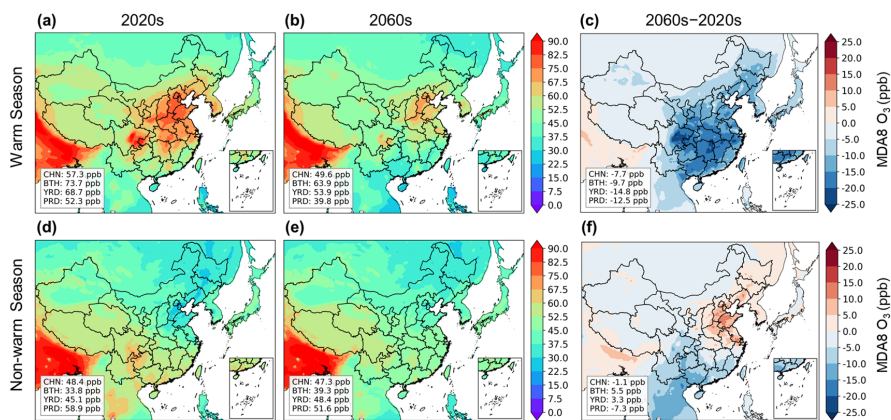
997 **Figure 2**



998
999



1000 **Figure 3**

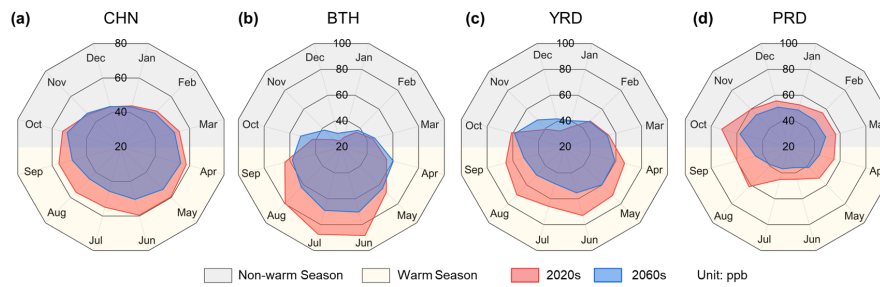


1001

1002



1003 **Figure 4**

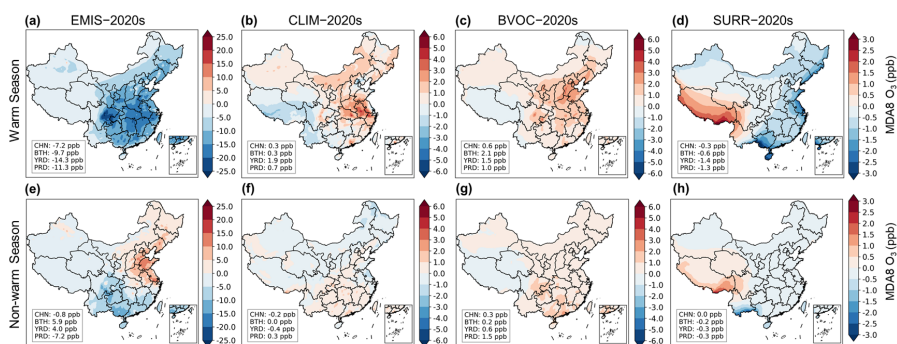


1004

1005



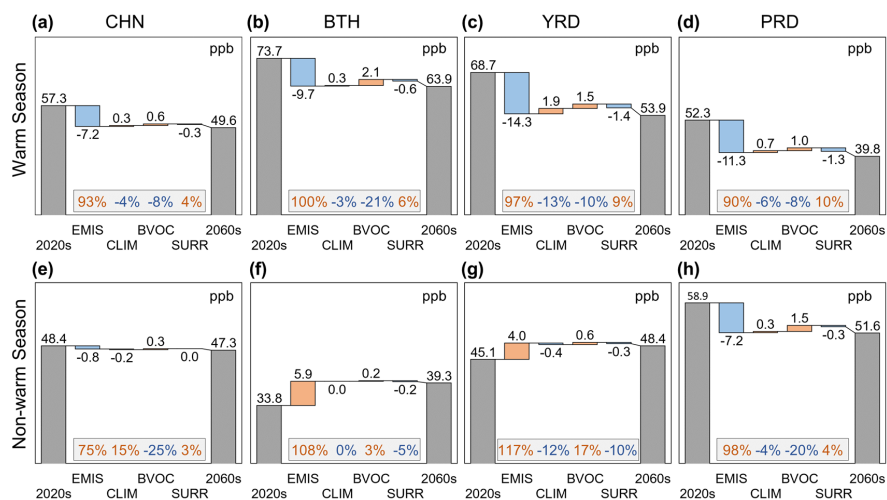
1006 **Figure 5**



1007
1008



1009 **Figure 6**

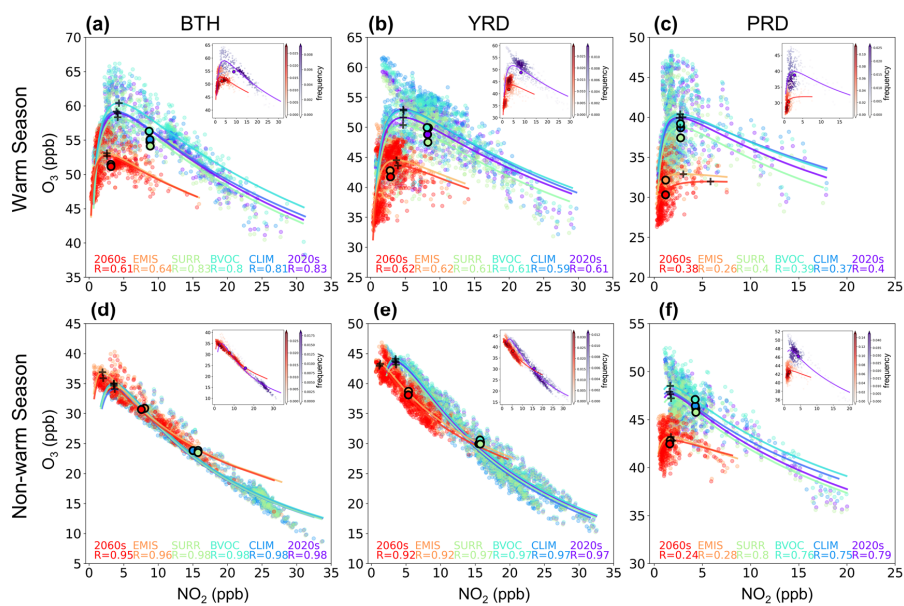


1010

1011



1012 **Figure 7**



1013
1014



1015 **Figure 8**

